Mathematical Modeling of Charged Laminate Materials

A Major Qualifying Project

submitted to the Faculty of the

WORCESTER POLYTECHNIC INSTITUTE

in partial fulfillment of the requirements for the Degree of Bachelor of Science

---

by Daniel Gendin

Mechanical Engeneering and Mathematical Sciences

Class of 2015

Advisor: Professor Burt Tilley

Executive Summary

Laminate materials are common in both biological and industrial applications. Of particular interest are charged laminates, a class of materials that is composed of charged solid layers and an interstitial fluid. Some examples of charged laminates are clays and cartilage. However, relatively few models exist to model the behavior of charged laminates. In this project we develop a mathematical model for the behavior of charged laminates. We model the material as a set of charged plates with a fluid between them. The material is analyzed in static equilibrium where the electrostatic forces between the plates must be balanced by the force of gravity, the internal capillary force, and the applied compressive load. We model the material as a continuum with infinitely many differentially close plates. The result is a nonlinear integral equation for the function that describes the spacing between plates. An analytical result for the resulting integral equation is obtained for the case when gravity and capillary forces are neglected. This result is than used to obtain approximate results for the more complicated cases where gravity and capillary forces are considered. The resulting spacing function is then used to obtain a stress strain relation for the material. The stress-strain results were than compared to experimental results with accuracy ranging from 5% to 19%.

Acknowledgments

I would like to thank Professor Tilley for providing the topic as well as for his guidance, support, and advice during each stage of this project.

Contents

List of Figures

1 Introduction

Most introductory engineering classes look at the behavior of pure materials [18]. The students calculate the stresses on an I-Beam made of pure steel or look at the strains in a pipe made of pure aluminum. These problems are useful for providing a rudimentary understanding of basic engineering concepts, however there exist few applications that use only pure materials, especially ones that are isotropic and linear-elastic. In modern mechanics, the supreme majority of materials used are a combination of different materials that were combined though layering, adding pores and inclusions, and other micro-mechanical methods, in order to obtain a material with the desired properties [15]. While being able to create a material with virtually any set of properties is a tantalizing prospect, predicting how a certain combination of materials act is a non trivial matter. In order to describe the behavior of a compound material one must look at the interactions between the components and think about which internal and external forces affect the behavior of the material and which ones can be neglected.

The commonality of non-homogeneous materials leads to a need to determine behaviors and effective material properties for these materials. Thus, in theoretical mechanics, problems of mathematical modeling of materials are exceptionally important. These problems allow one to apply the theories of classical mechanics to non-classical materials. A large variety of work has been done on the subject looking at how a material is affected by defects [27], inclusions [16], and layers of other materials [5].

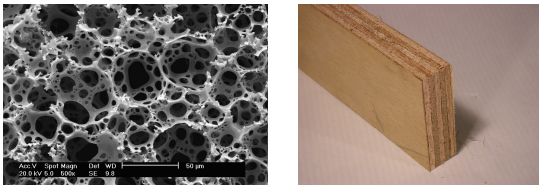

(a) Diagram of porous material [45]

(b) Plywood: Layered Material [14]

Figure 1: Examples of inhomogeneous materials

Much work has also been done on the subject of swelling and looking at the interaction of solids and fluids [19]. While a large amount of unique work has been done in the field of theoretical modeling of materials there are still many unsolved problems in it.

Of particular interest to us, in this project, is the modeling of a class of materials called laminates, meaning materials which are comprised of several layers. Laminate materials are ubiquitous and are used for a wide variety of purposes. Some common examples include: roads [1], which need to be both flexible, to avoid breaking due to thermal stresses, and firm , to resist deformation due to the weight of the cars. Automobile clutches [41]: which use a variety of solid and fluid layers to change the gear on a car. Tank Armor [33]: which uses a combination of flexible layers, firm layers, and even explosive layers to prevent a shell from penetrating the tank hull.

(a) Road Layers [34] (b) Automobile Clutch [3] (c) Tank Armor [23]

Figure 2: Examples of common laminates

Other common examples of laminates are biological materials. Since the 1990s there has been much research devoted to modeling and determining the properties of biological materials [24]. Using the methods of mechanics one is able to study and model materials that occur in nature as well as design materials that mimic the structures and functions of natural materials. Many biological materials exhibit laminate behavior. Materials, like bone, are laminate due to the way they form and grow, new layers of bone form directly on top of old layers causing bone to have a laminate structure [43]. Another example of a biological laminate material is the annulus fibrosis, which is a multilayer material that makes up part of the inter-vertebral disk, a soft tissue that transmits loads between vertebrae and allows for motion of the spine. The annulus fibrosis is layered in nature

and when a replacement for it is manufactured that material also has a layered structure [28]. Both biological and manufactured examples of laminate materials are extremely commonplace thus the ability to model them would be greatly beneficial.

While laminate materials are exceptionally common, there is no unified theory that explains the behavior of all classes of laminate materials. One of the earliest works in modeling laminate materials, and the earliest work on laminate plates, was done by Biot in 1957 [6]. In his paper, Biot performed analysis on a material composed entirely of solid layers, by using the methods of classical continuum mechanics. In 1973, Biot expanded his work by looking at the effects of an initial stress on the properties of a layered material [7]. This addition allowed for the modeling of simple laminates not only under compression and tension but also under vibration and buckling as well. In 1974 Charles W. Bert and Philip H. Francis wrote a paper in which they summarized the general state of the field of laminate materials including laminated bars, laminated plates, laminated shells, and sandwich structures [4]. The paper serves as a good reference about the behaviors of common, solid laminate structures, however, it by no means provides a complete description of the field of laminate materials. In 1989, Seale and Kausel wrote a paper in which, they used the theory of laminate materials and specifically the work done by Biot to model the behavior of soil [37]. They argued that their model is valid due to the strong effect of gravity on soil. Both static and dynamic loads were considered as well as isotropic and anisotropic media. In 1993, Ogden and Roxburgh wrote a paper in which, they looked at the effect of vibrations on deformations and stability of a material consisting of incompressible elastic plates [29]. The next year the same authors extended their results to compressible plates[35]. In 2005, Chakraborty, Gopalakrishnan, and Kausel published a paper where they analyzed wave propagation through a three-dimensional charged medium by viewing the medium as a combination of thin layers [11]. Overall, a limitation of the work that has been done is the lack of theoretical results for materials with both solid and liquid layers, results for charged

materials are also fairly rare.

In this project, we analyze the behavior of charged laminate materials. We look at how the internal electrostatic forces affect the material properties and how the behavior of the internal fluid layers affect the behavior of the material as a whole. A common example of such a material comes from biology, it is cartilage. According to [26] as well as [42], cartilage can be modeled as a pair of negatively charged plates with an uncharged layer of fluid in the middle.

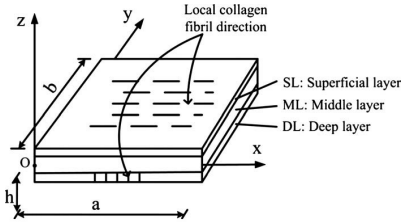

Figure 3: Cartilage Layers Diagram [42]

The dominant internal force that leads to deformation in the cartilage is electrostatic. Cartilage is exceptionally common in the human body, especially in children, as it is one of the main tissues in the formation of new bone [8]. Thus, the ability to model it and predict its behavior under load would be useful.

Another common charged laminate material is clay [30]. According to a 1989 [40]clays are composed of charged layers and the dominant internal force in clays is electrostatic repulsion .

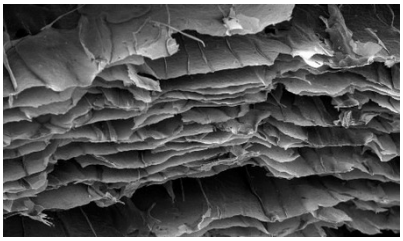

Figure 4: Clay Layers Diagram [22]

In accordance to Spitzer's article, as well as Mow's article, we model charged laminates as a set of charged plates. However, both articles approached the behavior of charged

laminates by looking at only two plates where in our analysis we look at a set of many plates. Also, Spitzer approached the problem from a chemical point of view while we are going to analyze the behavior of charged laminates mechanically.

Before we begin our analysis, we must first acknowledge some potential difficulties which research shows are inherent to the analysis of laminate materials. Firstly, laminate materials are prone to instability. This has been shown both theoretically [17] and experimentally [10]. We must thus acknowledge that our results are also prone to instability or else they would not serve as a proper model. Also, surprisingly little data exists on the shear properties and behavior of laminate materials, thus , like most of the found sources, we focus on longitudinal loading and properties.

2 Model

2.1 Problem Formulation

Consider a material with multiple charged layers. The layers are assumed to be thin disks surrounded by a fluid, that we assume is a pure dielectric, for the sake of simplicity. Each disk has a constant charge density of q, an area of A. The material is loaded by a force Nnormal to it's surface. We are concerned with how the material behaves and how this behavior is affected by the spacing between the laminates. In addition to the spacing, we are interested in obtaining a stress-strain curve for the material being modeled, where stress is defined as the load scaled with the cross sectional area($\sigma = \frac{N}{A}$), and strain is the deformation scaled with initial length($\epsilon = \frac{\Delta L}{L_0}$) and initial length is defined as the length at the point when load is 0.

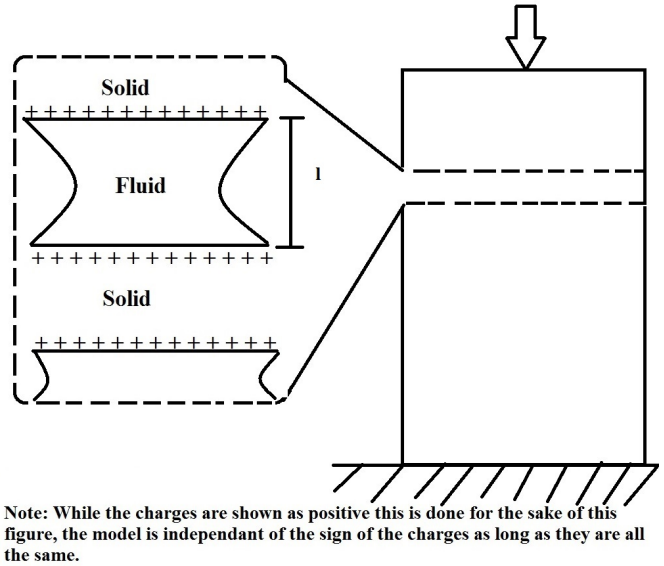

Figure 5: General Illustration of the material being modeled with several differentially small layers being shown.

2.2 Developing the Full Equation

We consider the effects of three forces in describing the system: electrostatic repulsion, gravity, and surface tension or capillary force. The effects of electrostatic repulsion are calculated in accordance to Coulomb's law, shown below,

$$F = -\frac{kQ_1Q_2}{l^2}. \tag{1}$$

Q represents the charge and l is the distance between the plates. For gravity, we simply consider the compression applied to a given layer by the layers above it. Lastly the force due to capillarity is calculated as

$$F = \frac{2\gamma A\cos(\theta)}{l}. \tag{2}$$

Where γ is the free surface energy (a material property) and θ is the contact angle, which is assumed constant for this model. In order to write our model we use the method of

cutoff length: meaning the spacing at height z is be denoted as $l(z)$. At heights close to z the spacing is assumed to just be $l(z)$ while at heights $\bar{z}$ far from z the spacing is $|z - \bar{z}|$.

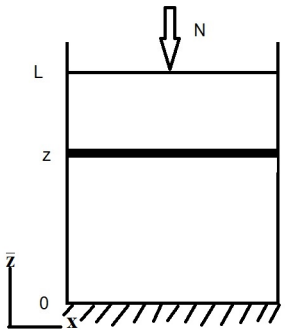

Figure 6: Illustration of continuum

We next say that for any z the compressive load must be balanced by the average net force due to the effects of electrostatics between the layer at z and the layers above it, the electrostatics between z and the layers close to it, and the electrostatics between the layer at z and the layers below it. Thus we obtain the following integral equation for the spacing function, $l(z)$

$$\begin{aligned} N = \frac{kq^2A^2}{L}\bigg(\int_0^{z-\frac{l(z)}{2}} \frac{1}{(z-\bar{z})^2}d\bar{z} + \int_{z-\frac{l(z)}{2}}^{z+\frac{l(z)}{2}} \frac{1}{l^2(z)}d\bar{z} + \int_{z+\frac{l(z)}{2}}^{L} \frac{1}{(z-\bar{z})^2}d\bar{z}\bigg) \\ - \frac{1}{L}g\bigg(\int_z^L (\rho_{\text{fluid}}l(z) + \rho_{\text{solid}}C)Adz\bigg) - \frac{1}{L}\int_0^L \frac{2\gamma A cos(\theta)}{l(z)}dz \end{aligned} \tag{3}$$

with the boundery conditions

$$l(0) = l(L) = 0, \tag{4}$$

where N is the magnitude of the compressive force, L is the total height of the material,ρ is the density, and C is the thickness of the solid layers.

The equation is non-dimensionalized and scaled with electrostatics (the dominant internal

force), and thus we obtain:

$$P = \int_0^{\zeta - \frac{l(\zeta)}{2}} \frac{1}{(\zeta - \bar{\zeta})^2} d\bar{\zeta} + \int_{\zeta - \frac{l(\zeta)}{2}}^{\zeta + \frac{l(\zeta)}{2}} \frac{1}{l^2(\zeta)} d\bar{\zeta} + \int_{\zeta + \frac{l(\zeta)}{2}}^{1} \frac{1}{(\zeta - \bar{\zeta})^2} d\bar{\zeta} \\ -G\rho\phi(1-\zeta) - G\int_{\zeta}^{1} l(\bar{\zeta}) d\bar{\zeta} - \Omega \int_0^1 \frac{1}{l(\zeta)} d\zeta \tag{5}$$

where

$$P = \frac{NL^2}{kq^2A^2}, \zeta = \frac{z}{L}, l(\zeta) = \frac{l(z)}{L}, G = \frac{\rho_{\text{fluid}} g L^2}{Lkq^2A}, \phi = \frac{c}{L}$$

thus ϕ is the solid fraction of the material,

$$\Omega = \frac{\gamma cos(\theta) A}{L} \cdot \frac{L^2}{kq^2A^2}, \rho = \frac{\rho_{\text{solid}}}{\rho_{\text{fluid}}}.$$

3 Solution of Equation

3.1 $G = \Omega = 0$: Electrostatic Forces Only

We begin our analysis of the system by just solving the simplest case, where electrostatic repulsion is the only internal force whose effects are considered.

$$P = \int_0^{\zeta - \frac{l(\zeta)}{2}} \frac{1}{(\zeta - \bar{\zeta})^2} d\bar{\zeta} + \int_{\zeta - \frac{l(\zeta)}{2}}^{\zeta + \frac{l(\zeta)}{2}} \frac{1}{l^2(\zeta)} d\bar{\zeta} + \int_{\zeta + \frac{l(\zeta)}{2}}^{1} \frac{1}{(\zeta - \bar{\zeta})^2} d\bar{\zeta}. \tag{6}$$

The equation can be solved analytically and thus we obtain an expression for our spacing function :

$$l(\zeta) = \frac{5\zeta^2 - 5\zeta}{P\zeta^2 - P\zeta - 1}. \tag{7}$$

A plot of the function is shown in Figure 7.

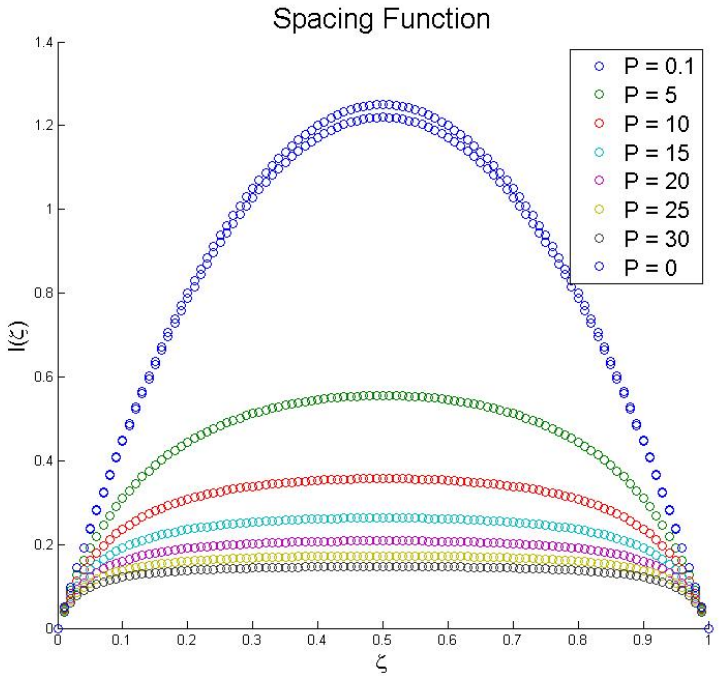

Figure 7: Spacing function for various values of P

As expected, the spacing function is symmetric and maximum at the center. Also these results seem to match our physical intuitions, as expected an increase in force leads to a decrease in spacing. However, one piece of the data appears counter-intuitive. A finite result is obtained when the load is zero, however, according to Earnshaw's Theorem [13], the plate should be pushed apart an infinite distance if there is no constraining force. The reason for the finite spacing distribution is the fact that the spacing is finite is due to the fact that the spacing was scaled with the total material length, thus an infinite spacing is being divided by an infinite length and a seemingly finite result is being obtained, however if we were to look at the non-scaled solution it would diverge as expected.

3.2 Solution Including Gravity

The equation which considers gravity but not capillarity is:

$$P = \int_0^{\zeta - \frac{l(\zeta)}{2}} \frac{1}{(\zeta - \bar{\zeta})^2} d\bar{\zeta} + \int_{\zeta - \frac{l(\zeta)}{2}}^{\zeta + \frac{l(\zeta)}{2}} \frac{1}{l^2(\zeta)} d\bar{\zeta} + \int_{\zeta + \frac{l(\zeta)}{2}}^{1} \frac{1}{(\zeta - \bar{\zeta})^2} d\bar{\zeta} - G \int_{\zeta}^{1} (l(\bar{\zeta}) + \rho\phi) d\bar{\zeta} \quad (8)$$

After some simplification the equation becomes:

$$P = \frac{5}{l(\zeta)} - \frac{1}{\zeta} + \frac{1}{\zeta - 1} - G\rho\phi(1 - \zeta) - G \int_{\zeta}^{1} l(\bar{\zeta}) d\bar{\zeta} \quad (9)$$

This equation can not be solved analytically and thus we apply a numerical approach. Let us partition ζ such that $\zeta_1 = 0, \zeta_1 = \Delta\zeta, \zeta_2 = 2\Delta\zeta, ...\zeta_N = 1$. We now wish to determine the spacing at every $\zeta_i, i = 1, 2, ...N$. We replace the integral with a quadrature rule. Our equation thus becomes

$$P = \frac{5}{l_i} - \frac{1}{\zeta_i} + \frac{1}{\zeta_i - 1} - G\rho\phi(1 - \zeta_i) - G \cdot \Delta\zeta \cdot \sum_{j=i}^{N} w_{ij} l_j, i = 2, ..., N - 1. \quad (10)$$

Where $l_i = l(\zeta_i)$ and w_{ij} is the quadrature for trapezoidal rule. Starting at $i = N$ and iterating backwards, one can obtain a system of N quadratic equations for every l. Assuming that $l_1 = l_N = 0$ one can first obtain l_{N-1} and then l_{N-2} using the previous result, and so on and so forth. Results are shown in Figures 8 and 9 below.

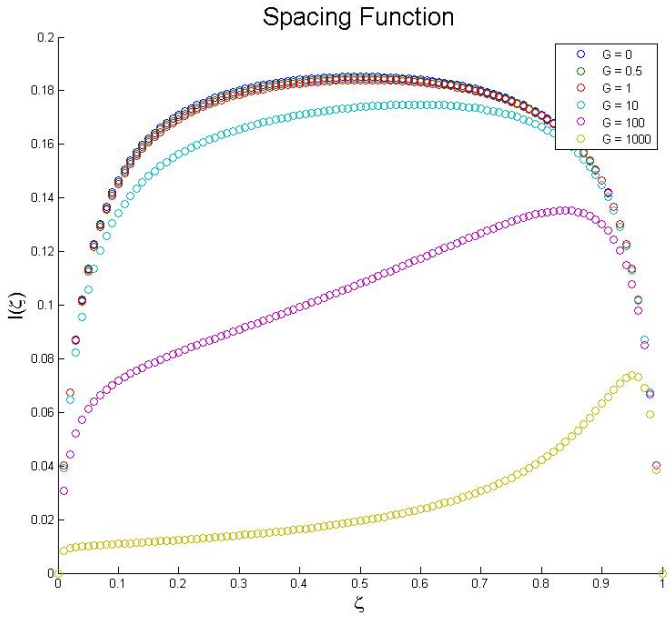

Figure 8: Spacing function for various G. $P = 23$, $\rho = 1$, $\phi = 0.5$

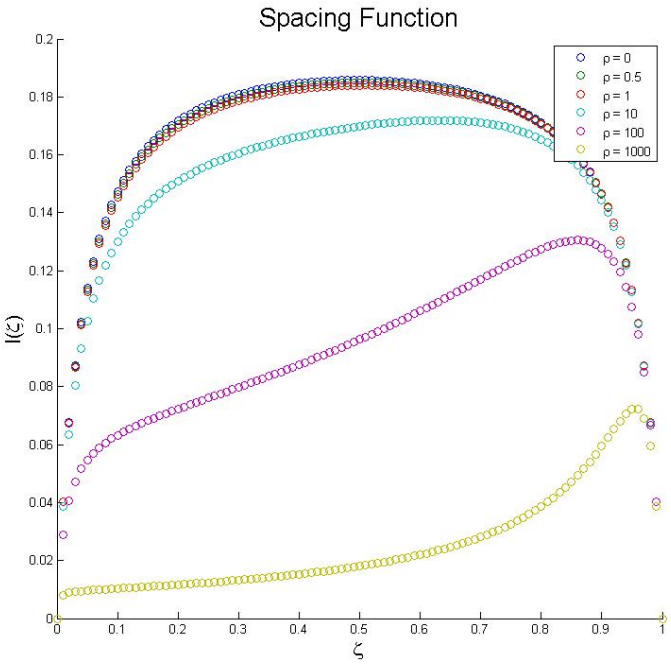

Figure 9: Spacing function for various ρ. $P = 23$, $G = 1$, $\phi = 1$

The results obtained again seem to match our physical intuitions as an increase in the gravitational pull or the density of the solid compared to the liquid led to a decrease

in spacing. This is because an increased gravitational force or heavier plates lead to a greater compressive force applied to every layer. Also, the spacing at the bottom is smaller than the spacing at the top [39], this is consistent with our physical intuition as the bottom layers would be more compressed than the top layers since more weight is applied to the bottom layers than the top.

3.3 Solution of the Full System

We finally consider the full system that was presented in equation (5). The system is simplified and becomes:

$$P = \frac{5}{l(\zeta)} - \frac{1}{\zeta} + \frac{1}{\zeta - 1} - G\rho\phi(1-\zeta) - G\int_{\zeta}^{1} l(\bar{\zeta})d\bar{\zeta} - \Omega\int_{0}^{1}\frac{1}{l(\zeta)}d\zeta. \tag{11}$$

Again this equation can not be solved analytically thus we partition our interval into a finite number of parts and replace the integrals with quadrature rules.

$$P = \frac{5}{l_i} - \frac{1}{\zeta_i} + \frac{1}{\zeta_i - 1} - G\rho\phi(1-\zeta_i) - G\cdot\Delta\zeta\cdot\sum_{j=i}^{N} w_{ij}l_j - \Omega\sum_{j=1}^{N}\frac{w_{ij}\Delta\zeta}{l_k}, i = 2, ..., N-1. \tag{12}$$

Let

$$u = \begin{pmatrix} l_1 \\ l_2 \\ \vdots \\ l_N \end{pmatrix}, v = \begin{pmatrix} \frac{1}{l_1} \\ \frac{1}{l_2} \\ \vdots \\ \frac{1}{l_N} \end{pmatrix}$$

, then (12) can be rewritten as:

$$\underline{\underline{A}}\,\underline{u} + \underline{\underline{B}}\,\underline{v} = \underline{C} \tag{13}$$

where

$$A_{ij} = \begin{cases} 0 & i > j \\ -Gw_{ij}\Delta\zeta & j \geq i \end{cases} \tag{14}$$

$$B_{ij} = \begin{cases} -\Omega w_{ij}\Delta\zeta & i \neq j \\ -\Omega w_{ij}\Delta\zeta + 5 & i = j \end{cases} \tag{15}$$

$$C_i = P + \frac{1}{\zeta_i} - \frac{1}{\zeta_i - 1} + G\rho\phi(1 - \zeta_i), i = 2, ..., N - 1 \tag{16}$$

A variation of Gauss-Seidel method [9] is used to solve this system. We make an initial guess, in our case we use the solution for equation (10) as an initial guess for $\vec{u}$ and the reciprocal of this as the initial guess for $\vec{v}$. We then assume all the values of u are know except for one and compute that value of u_i we then set u_i equal to the new obtained value and go on to compute the value of u_{i+1}. This process is repeated cyclically for all values of u until the results are within a fixed value (1%) of each other.

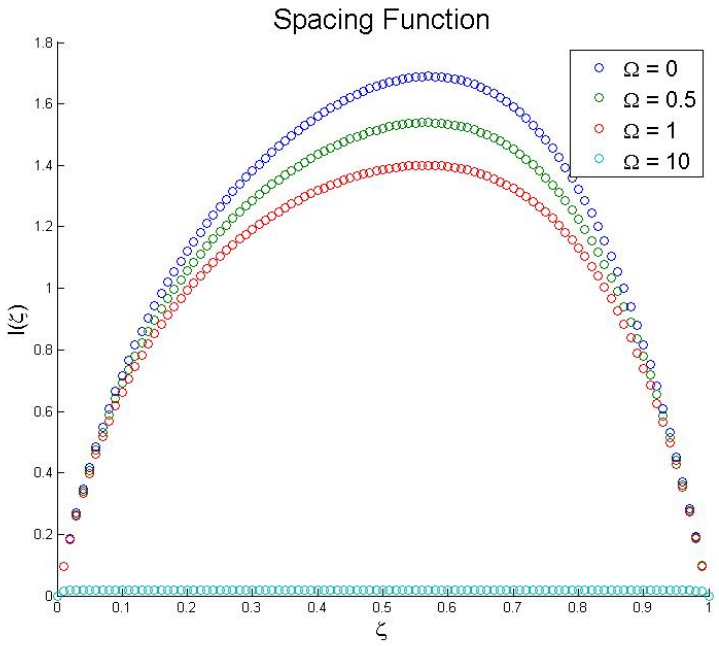

Figure 10: Spacing function for various values of Ω.$G = 1$, $P = 1$, $\rho = 1.5$, $\phi = 0.5$

Again,the results appear to match our physical intuition as the surface tension acts to prevent the fluid from being stretched, thus a larger value of surface tension leads to a smaller spacing distribution.

3.3.1 Validation With Fixed Point Method

In order to validate the results we obtained from the Gauss-Seidel method we compare them to results obtained through the fixed-point method. We take the system from (13) and solve it by selecting an initial guess for $\vec{u}$ and $\vec{v}$ and using those initial guesses to solve the system iteratively, selecting every next $\vec{v}$ by

$$\underline{v} = \underline{\underline{B^{-1}}}\,(\underline{C} - \underline{\underline{A}}\,\underline{u}). \tag{17}$$

This method converges fairly quickly and appears to agree with the results obtained through Gauss-Seidel, suggesting that the results for spacing function that have been obtained are valid.

3.4 Stress-Strain Relation

Now that we have fully described the behavior of the given system we wish to obtain a stress-strain relation from the results. In order to do so, we need to rescale the system with undeformed length rather than total length.The system thus becomes

$$\begin{aligned} P = \int_0^{\zeta - \frac{l(\zeta)}{2}} \frac{1+\epsilon}{(\zeta-\bar{\zeta})^2} d\bar{\zeta} + \int_{\zeta-\frac{l(\zeta)}{2}}^{\zeta+\frac{l(\zeta)}{2}} \frac{1}{l^2(\zeta)} d\bar{\zeta} + \int_{\zeta+\frac{l(\zeta)}{2}}^{1} \frac{1}{(\zeta-\bar{\zeta})^2} d\bar{\zeta} \\ -G\rho\phi(1+\epsilon-\zeta) - G\int_{\zeta}^{1+\epsilon} l(\bar{\zeta}) d\bar{\zeta} - \Omega \int_0^{1+\epsilon} \frac{1}{l(\zeta)} d\zeta. \end{aligned} \tag{18}$$

The physical definition of spacing and length lead to the following system of equations.

$$\phi + \int_0^1 l d\zeta = 1 + \epsilon \tag{19}$$

$$\phi + \int_0^1 l_0 d\zeta = 1 \tag{20}$$

Combining (18) and (19) we obtain

$$\epsilon = \int_0^1 l d\zeta - \int_0^1 l_0 d\zeta \tag{21}$$

we approximate the integrals with quadrature rules and obtain

$$\epsilon = \sum_{j=1}^{N} w_j l \Delta\zeta - \sum_{j=1}^{N} w_j l_0 \Delta\zeta. \tag{22}$$

Thus, for any given load, we can obtain a spacing and use that spacing to obtain a strain. Results for the stress-strain relation are presented in Figure 11.

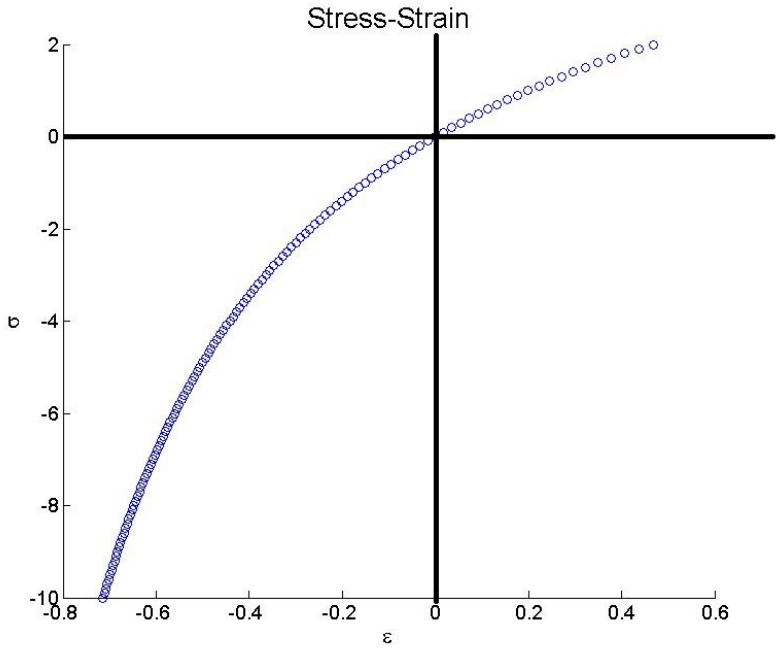

Figure 11: Stress-Strain Relation

The result for the stress strain relation fits our physical intuition, if we think of the system as a set of charged plates, for compression, eventually the plates are pushed so close together that electrostatic repulsion dominates such that it takes a larger change in load to enact a small deformation. On the other hand, for tension, at one point the plates are far enough apart that even a small change in load leads to large deformations.

4 Validation

4.1 Comparison to Experimental Results

In order to validate the model we compare our theoretical results to experimental results for both clay(Kaolinite) and cartilage (Articular Cartilage). The results of our comparison are presented in Figure 12.

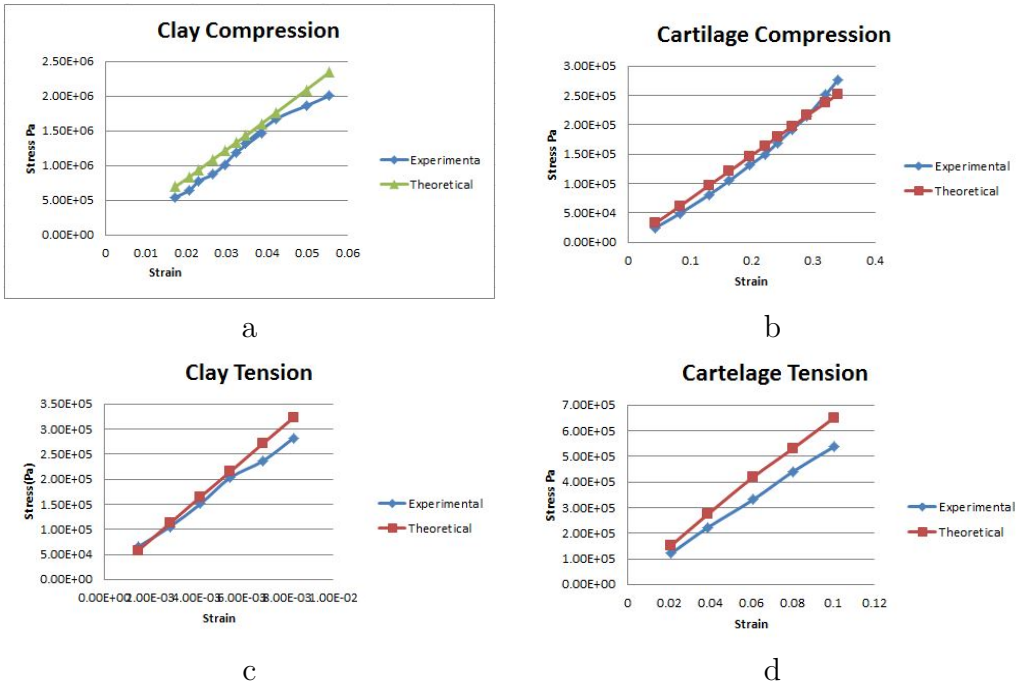

Figure 12: Experimental and theoretical comparison: **a.** Average difference: 14.1% data from Illampas, Ioannou, and Charmpis 2014 [20], **b.** Average difference: 10.6% data from Schinagl, Gurskis, Chen, and Sah 1997 [36], **c.** Average difference: 5.56% data from Kavak and Baykal 2014 [21], **d.** Average difference: 18.9% data from Mow, Holmes, and Lai 1984[26]

The values of the parameters were chosen from physically realistic values in order to best fit the experimental results. The physically realistic values for clays are: $-0.027C \leq q \leq -0.038C$[46], $1200\frac{kg}{m^3} \leq \rho_{solid} \leq 1600\frac{kg}{m^3}$ [2], $0.17 \leq \phi \leq 0.82$ [32], $17.8 \leq \theta \leq 55.7$ [38]. The values of the parameters that were used when comparing to the experimental data which seemed to produce the best results are: $q = -0.027C, \rho_{fluid} = 1000\frac{kg}{m^3}, \rho_{solid} =$

$1500\frac{kg}{m^3}, \phi = 0.2, \theta = 40°, \gamma = 0.072$

For cartilage the values are: $q = 0.037 \pm 0.004\frac{C}{m^2}$ [25], $\rho_{solid} = 250\frac{kg}{m^3}$ [44], $0.4 \leq \phi \leq 0.6$ [31], and $\theta = 80 \pm 0.5$ [12]. The values of the parameters that were used when comparing to the experimental data which seemed to produce the best results are: $q = -0.037C, \rho_{fluid} = 1000\frac{kg}{m^3}, \rho_{solid} = 250\frac{kg}{m^3}, \phi = 0.5, \theta = 80°, \gamma = 0.072$

Overall, our model appears to be a good fit for the behavior of the material that was found experimentally. An interesting observation is that our model appears to overestimate the experimental results for stress for any given strain. The reasons for this are not immediately clear from the model and should be investigated further. It should also be notedthat these results are extremely sensetive to changes in the vlaue of q, this is an example of the previously discussed instability inherent to laminate materials.

5 Conclusion

During the course of this project, we developed an equation that describes the behavior of charged laminates. We then used analytical and numerical methods in order to solve this equation and describe the spacing distribution of the material. This spacing distribution was then used to obtain a stress-strain relation for a given material. These theoretical results were compared to experimental results for tow distinct examples of charged laminates, cartilage and clay, these results appeared to correlate fairly well with ones obtained experimentally. This correlation provides the tools for future researchers and engineers to be able to predict the properties of clay, cartilage, or another charged laminate material based on the properties of this material. The results can be applied to both industrial applications, where clays and ceramic materials are common, or the results can be applied to the quickly growing field of biomaterials.

Future research in this area should begin by obtaining an analytical expression for the obtained stress-strain relation. More research should also be done on the internal

forces that may need to be added to the model in order to increase its accuracy. Lastly, it would be interesting to weaken the requirement that the interstitial fluid be a pure dielectric.

6 Appendices

6.1 Appendix 1: Error due to increment size

In order to make sure that the obtained results are valid, we should make sure that the error caused by the spacing size. An error can be considered small if it is equally or less significant than the error being caused by the trapezoid rule we used to approximate the integral. The logarithm base 10 of the difference in spacing function caused by different partitions is plotted below.

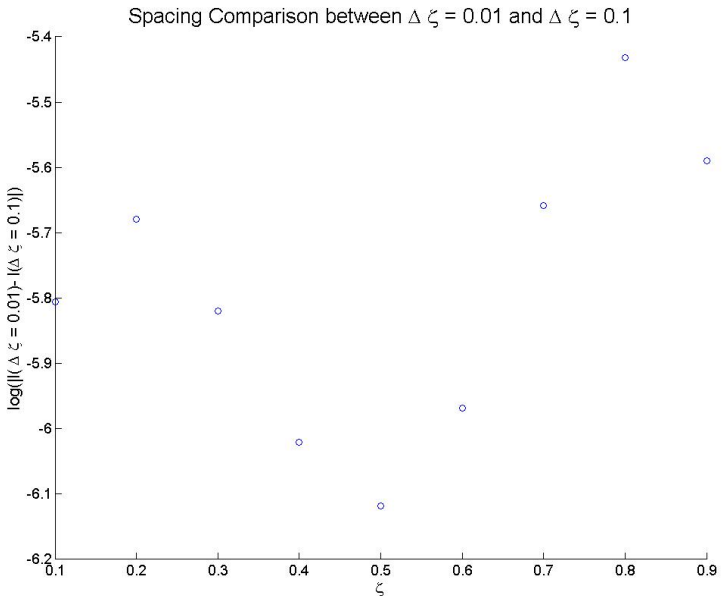

Figure 13: Effect of partition size on error.

The error caused by the partition is on the order of 10^{-6} where as the error caused by trapezoidal rule is on the order of $\frac{1}{n^2}$ or in this case 10^{-4}, which is significantly bigger.

Thus we can view the error that is caused by the increment size as negligibly small. If we do need more accuracy we should look into a more accurate quadrature rule.

6.2 Appendix 2: Matlab Code

6.2.1 Code for Solution of Pure Electrostatics

```
function l = lo (F, z)
l = (5 * z^2 - 5*z)/ (F*z^2-F*z-1);
```

6.2.2 Code for Solution of System including Gravity

```
function l = ToyMass(G, p,cb, F, dz)
 z = (0:dz:1)';
 l = zeros(size(z));
 sizevec = size(z);
 n = sizevec(1);
 i = n-1;
 while i > 1
 sum = 0;
     for k = i+1 : n
         w = 1;
         if(or(k==i+1,k==n))
            w = 0.5;
         end
        sum = sum + w*l(k);
     end
     a = G*dz;
     b = F - 1 / (z(i)-1) + 1 / z(i) + G*p*cb*(1-z(i)) - sum*G*dz;
     c = -5;
```

```
19       l(i) = (-b + sqrt(b^2 - 4*a*c))/(2*a);
20       i = i - 1;
21   end
22   lorig = zeros (size (n));
23    for i = 1 : length (z);
24      lorig(i) = lo(F, z(i));
25    end
```

6.2.3 Code for Solution of Full System

```
1  function [u,A,B,C,ut] = Capilary2(O,G,p,cb,F,dz)
2  %z = (0:dz:1)';
3  z = (0:dz:1)';
4  n = length(z);
5  u = ToyMass(G,p,cb,F,dz);
6  ut = u;
7  %disp("found u")
8  %[A][u]+[B][v] = [C]
9  A = zeros(n,n);
10 B = zeros(n,n);
11 C = zeros(n,1);
12 size(A)
13 for i = 2:n-1
14     C(i) = F + 1/(z(i)) -1/(z(i)-1)+G*p*cb*(1-z(i));
15 end
16 C(1) = F;
17 C(n) = F;
18 for i = 1:n
19    for j = 1 :n
20       if j < i
21          A(i,j) = 0;
```

```
22        end
23        if j ≥ i
24             w = 1;
25           if(or(j==i+1,j==n))
26              w = 0.5;
27           end
28           A(i,j) = -G*dz*w;
29        end
30     end
31  end
32  %disp("found A")
33  for i = 1:n
34     for j = 1:n
35           w = 1;
36           if(or(j==2,j==n))
37              w = 0.5;
38           end
39           B(i,j) = -O*dz*w;
40
41     end
42  end
43  %disp("found B")
44  tf = 0;
45  newtot=1;
46  oldtot = 1;
47  while tf == 0
48     for i = 2 : n-1
49        sum = 0;
50        for j = 2:n-1
51           if i≠j
52               sum = sum + A(i , j)*u(j)+B(i,j)/(u(j));
53           end
54        end
```

```
55        c = C(i)-sum;
56        a = A(i,i);
57        b = B(i,i)+5;
58        u(i) = (c - sqrt(c^2-4*a*b))/(2*a);
59     end
60     for i = 1 : 1 : size(u)
61     newtot = newtot + u(i);
62     end
63     check = (newtot-oldtot)/oldtot
64     if (newtot - oldtot)/oldtot ≤ 0.01
65        tf = 1;
66     end
67     oldtot = newtot;
68  end
69  size(A);
70  B=B+5*eye(n);
71  return
```

6.2.4 Code for Fixed Point Iteration

```
1  clf;
2  %Capilary(O,G,p,cb,F,dz)
3   z = (0:0.01:1)';n=length(z);
4   A0=zeros(n,n);B0=A0;C0=zeros(n,1);
5      [l0,A0,B0,C0,lg] = Capilary2(1,1,1.5,.5, 0,0.01);
6    u=l0(2:end-1);A=A0(2:end-1,2:end-1);B=B0(2:end-1,2:end-1);
7    C = C0(2:end-1);
8   norm(A*u+B*(1./u)-C)
9  %
10 % check with fixed point
11 %
```

```
u1 = lg(2:end-1);
U = u1;
for it = 1:8
  v2 = B\(C-A*u1);
  u2=1./v2;
  U = [U u2];
  if it ==1
  unorm=norm(u2-u1);
  else
  unorm=[unorm norm(u2-u1)]
  u1=u2;
  end
end
```

6.2.5 Code for Stress-Strain

```
function e = StressStrain(O, G, p, cb,dz,df)
F = [-10: df: 2];
L0 = sum(Capilary2(O, G, p, cb, 0, dz));
e = zeros(size(F));
for i = 1:1:length(F)
    L = sum(Capilary2(O, G, p, cb, -1*F(i), dz));
    e(i) = (L-L0)*dz;
end
```

6.2.6 Code for Stress Strain Including Dimentional Parameters

```
function e = StressStraindim
clf
```

```
q = -0.037; %C
A = 1;
L = 1;
k = 9*10^9;
g = 9.8;
pf = 1000;
ps = 250;
cb = 0.5;
gamma = 0.072;
dz= 0.01;
df = 100;
s = [0:df:73000];

O = gamma*A*cos(80*pi/180)/L*(L^2)/(k*(q^2)*(A^2));
p = ps/pf;
F = zeros(size(s));
for i = 1 :1: length(s)
    F(i) = s(i)*L^2 / (k*q^2 * A);
end
G = pf*g*L/(k*q^2*A^2);

L0 = sum(Capilary2(O, G, p, cb, 0, dz));
e = zeros(size(F));
for i = 1:1:length(F)
     L = sum(Capilary2(O, G, p, cb, -F(i), dz));
     e(i) = (L-L0)*dz;
end
scatter(e,s)
 xlabel('\epsilon', 'FontSize', 16)
 ylabel('\sigma(Pa)', 'FontSize', 16)
```

References

[1] Postconstruction environmental monitoring of a fly ash-based road subbase. *Practice Periodical on Structural Design and Construction*, 11(4):238–246, 2006.

[2] Earth or soil weigth and composition. `http://www.engineeringtoolbox.com`, 2015. Accesed: 4/27/2015.

[3] Ward Automotive. `http://www.wardautomotive.net/blog/bid/183763/The-top-5-things-that-can-go-wrong-with-your-car-s-clutch`. Accesed: 3/27/2015.

[4] Charles W Bert and Philip H Francis. Composite material mechanics: structural mechanics. *AIAA journal*, 12(9):1173–1186, 1974.

[5] M.A Biot. Continiuum dynamics of elastic plates and multilayeres solids under initial stress. *Journal of Mathematics and Mechanics*, 12(6):793–810, 1963.

[6] M.A Biot. A new approach to the mechanics of orthotropic multilayered plates. *International Journal of Solids and Structures*, 8(4):475–90, 1972.

[7] MA Biot. Buckling and dynamics of multilayered and laminated plates under initial stress. *International Journal of Solids and Structures*, 10(4):419–451, 1974.

[8] Encyclopaedia Britannica. Cartilage. `http://www.britannica.com/EBchecked/topic/97461/cartilage`, 2014. Accesed: 3/27/2015.

[9] R. Burden and J. Faires. *Numerical Analysis*. Cengage Learning, 2010.

[10] Martin Centurion, Mason A Porter, Ye Pu, PG Kevrekidis, DJ Frantzeskakis, and Demetri Psaltis. Modulational instability in a layered kerr medium: Theory and experiment. *Physical review letters*, 97(23):234101, 2006.

[11] A Chakraborty, S Gopalakrishnan, and E Kausel. Wave propagation analysis in inhomogeneous piezo-composite layer by the thin-layer method. *International journal for numerical methods in engineering*, 64(5):567–598, 2005.

[12] Jacques Chappuis, Igor A Sherman, and A Wilhelm Neumann. Surface tension of animal cartilage as it relates to friction in joints. *Annals of biomedical engineering*, 11(5):435–449, 1983.

[13] John Daintith. `http://app.knovel.com/hotlink/toc/id:kpDCE00011/dictionary-chemistry/dictionary-chemistry`, 2008.

[14] The Home Depot. Whole piece birch domestic plywood.

[15] Anders Doughett and Peder Asnarez. *Composite Laminates : Properties, Performance and Applications*. Material Science and Technologies Series. Nova Science Publishers, Inc, New York, 2010.

[16] Oleg Eroshkin and Igor Tsukrov. On micromechanical modeling of particulate composites with inclusions of various shapes. *International Journal of Solids and Structures*, 42(2):409–27, 2005.

[17] AN Guz. Constructing the three-dimensional theory of stability of deformable bodies. *International applied mechanics*, 37(1):1–37, 2001.

[18] RC Hibbeler. *Mechanics of Materials (2000)*. Prentice Hall, Upper Saddle River.

[19] Jacques M Huyghe and JD Janssen. Quadriphasic mechanics of swelling incompressible porous media. *International Journal of Engineering Science*, 35(8):793–802, 1997.

[20] Rogiros Illampas, Ioannis Ioannou, and Dimos C Charmpis. Adobe bricks under compression: Experimental investigation and derivation of stress–strain equation. *Construction and Building Materials*, 53:83–90, 2014.

[21] Aydın Kavak and Gökhan Baykal. Long-term behavior of lime-stabilized kaolinite clay. *Environmental earth sciences*, 66(7):1943–1955, 2012.

[22] John Mangels. Case western reserve university engineering professor transforms clay into high-tech material. `http://www.cleveland.com/science/index.ssf/2009/05/case_western_reserve_universit_7.html`, 2009. Accesed: 3/27/2015.

[23] Maybach. Chobham armor. `http://maybach300c.blogspot.com/2012/09/chobham-armor.html`, 2012. Accesed: 3/27/2015.

[24] Marc André Meyers, Po-Yu Chen, Albert Yu-Min Lin, and Yasuaki Seki. Biological materials: structure and mechanical properties. *Progress in Materials Science*, 53(1):1–206, 2008.

[25] A Minassian, D O'Hare, KH Parker, JPG Urban, K Warensjo, and CP Winlove. Measurement of the charge properties of articular cartilage by an electrokinetic method. *Journal of orthopaedic research*, 16(6):720–725, 1998.

[26] Van C Mow, Mark H Holmes, and W Michael Lai. Fluid transport and mechanical properties of articular cartilage: a review. *Journal of biomechanics*, 17(5):377–394, 1984.

[27] Toshio Mura. *Micromechanics of Defects in Solids*. The Hague: M. Nijhoff, 1982.

[28] Nandan L Nerurkar, Brendon M Baker, Sounok Sen, Emily E Wible, Dawn M Elliott, and Robert L Mauck. Nanofibrous biologic laminates replicate the form and function of the annulus fibrosus. *Nature materials*, 8(12):986–992, 2009.

[29] RW Ogden and DG Roxburgh. The effect of pre-stress on the vibration and stability of elastic plates. *International Journal of Engineering Science*, 31(12):1611–1639, 1993.

[30] Erwan Paineau, Isabelle Bihannic, Christophe Baravian, Adrian-Marie Philippe, Patrick Davidson, Pierre Levitz, Srgio S. Funari, Cyrille Rochas, and Laurent J. Michot. Aqueous suspensions of natural swelling clay minerals. 1. structure and electrostatic interactions. *Langmuir*, 27(9):5562–5573, 2011.

[31] S. Pal. *Design of Artificial Human Joints & Organs*. Springer, 2013.

[32] Angelica M Palomino, Susan E Burns, and J Carlos Santamarina. Mixtures of fine-grained minerals–kaolinite and carbonate grains. *Clays and Clay Minerals*, 56(6):599–611, 2008.

[33] Tim Ripley. New armour solutions. *Armada International*, 26(5):24–32, 2002.

[34] Weymouth Relief Road. Chalk testing. `https://weymouthreliefroad.wordpress.com/tag/road-layers/page/2/`. Accesed: 3/27/2015.

[35] DG Roxburgh and RW Ogden. Stability and vibration of pre-stressed compressible elastic plates. *International journal of engineering science*, 32(3):427–454, 1994.

[36] Robert M Schinagl, Donnell Gurskis, Albert C Chen, and Robert L Sah. Depth-dependent confined compression modulus of full-thickness bovine articular cartilage. *Journal of Orthopaedic Research*, 15(4):499–506, 1997.

[37] Sandra H Seale and Eduardo Kausel. Point loads in cross-anisotropic, layered half-spaces. *Journal of Engineering Mechanics*, 115(3):509–524, 1989.

[38] Jianying Shang, Markus Flury, James B Harsh, and Richard L Zollars. Comparison of different methods to measure contact angles of soil colloids. *Journal of colloid and interface science*, 328(2):299–307, 2008.

[39] Suresh C Sharma and Surendra RS Kafle. Effect of gravity on density distributions and orthopositronium annihilation rates in ethane and methane near the critical point. *The Journal of Chemical Physics*, 78(11):6897–6900, 1983.

[40] J. J. Spitzer. Electrostatic calculations on swelling pressures of clay-water dispersions. *Langmuir*, 5(1):199–205, 1989.

[41] K. Tripathi. A novel approach for enhancement of automobile clutch engagement quality using mechatronics based automated clutch system. *Journal of The Institution of Engineers (India): Series C*, 94(1):9–20, 2013.

[42] Leo Q Wan, X Edward Guo, and Van C Mow. A triphasic orthotropic laminate model for cartilage curling behavior: fixed charge density versus mechanical properties inhomogeneity. *Journal of biomechanical engineering*, 132(2):024504, 2010.

[43] K.R. Williams. *Interfaces in medicine and mechanics–2*. INTERFACES IN MEDICINE AND MECHANICS. Elsevier Applied Science, 1991.

[44] Marc Robin Anne Valle Chelsea Catania Patrick Legriel Grard Pehau-Arnaudet Florence Babonneau Marie-Madeleine Giraud-Guille Nadine Nassif Yan Wang, Thierry Azas. Comparison of collagen density and organization between in vitro models and bone. `http://www.nature.com/nmat/journal/v11/n8/fig_tab/nmat3362_F1.html`.

[45] Caroline M. Zeyfert. Pmse 307. `http://oasys2.confex.com/acs/238nm/techprogram/P1273327.HTM`, 2009. Accesed: 3/27/2015.

[46] Zhihong Zhou and William D Gunter. The nature of the surface charge of kaolinite. *Clays and Clay Minerals*, 40(3):365–368, 1992.